Inorganic Chemistry

Article

pubs.acs.org/IC

Thermoelectric Properties of Ag-Doped $Bi_2(Se,Te)_3$ Compounds: Dual Electronic Nature of Ag-Related Lattice Defects

Meng-Pei Lu,[†] Chien-Neng Liao,*[,†] Jing-Yi Huang,[‡] and Hung-Chang Hsu[‡]

[†]Department of Materials Science and Engineering, National Tsing Hua University, Hsinchu 30013, Taiwan

[‡]New Materials Research and Development Department, China Steel Corporation, Kaohsiung 81257, Taiwan

Supporting Information

ABSTRACT: Effects of Ag doping and thermal annealing temperature on thermoelectric transport properties of $Bi_2(Se,Te)_3$ compounds are investigated. On the basis of the comprehensive analysis of carrier concentration, Hall mobility, and lattice parameter, we identified two Ag-related interstitial (Ag_i) and substitutional (Ag_{Bi}) defects that modulate in different ways the thermoelectric properties of Ag-doped $Bi_2(Se,Te)_3$ compounds. When Ag content is less than 0.5 wt %, Ag_i plays an important role in stabilizing crystal structure and suppressing the formation of donor-like Te vacancy (V_{Te}) defects, leading to the decrease in carrier concentration with increasing Ag content. For the heavily doped $Bi_2(Se,Te)_3$ compounds (>0.5 wt % Ag), the increasing concentration of Ag_{Bi} is held responsible for the increase of electron concentration because formation of Ag_{Bi} defects is accompanied by annihilation of hole carriers. The analysis of Seebeck coefficients and temperature-dependent electrical properties suggests that electrons in Ag-doped $Bi_2(Se,Te)_3$ compounds are subject to a mixed mode of impurity scattering and lattice scattering. A 10% enhancement of thermoelectric figure-of-merit at room temperature was achieved for 1 wt % Ag-doped $Bi_2(Se,Te)_3$ as compared to pristine $Bi_2(Se,Te)_3$.

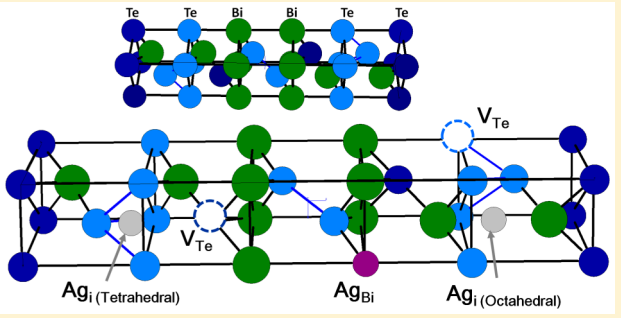

INTRODUCTION

Thermoelectric materials that enable direct conversion between heat and electricity are highly suitable for some unique applications such as waste heat recovery and precise temperature control.[1,2] To evaluate the performance of thermoelectric materials, a dimensionless parameter, so-called thermoelectric figure-of-merit, has been used and defined as $ZT = S^2T/\rho\kappa$, where S, ρ, κ, and T are Seebeck coefficient, electrical resistivity, thermal conductivity, and absolute temperature, respectively. Bismuth telluride-based compounds are the most well-known thermoelectric materials used in low-temperature cooling and generation devices. They possess a rhombohedral crystal structure with space group $R\bar{3}m$, which is usually described by a hexagonal cell with 15 atomic layers stacking in the direction of c-axis, as shown below.

$$\cdots Te^{(1)} - Bi - Te^{(2)} - Bi - Te^{(1)} \cdots Te^{(1)} - Bi - Te^{(2)} - Bi - Te^{(1)} \cdots Te^{(1)} - Bi - Te^{(2)} - Bi - Te^{(1)} \cdots$$

Note that $Te^{(1)}$ and $Te^{(2)}$ are nonequivalent Te lattice sites. The $Te^{(1)}$ atoms are weakly bonded to the neighboring $Te^{(1)}$ layer by a van der Waals force. Such a low-symmetry structure gives rise to highly anisotropic electrical and thermal transport properties.[3] Therefore, ZT maximization can be achieved by tailoring crystallographic texture of Bi−Te-based compounds.[4−7] Aside from texture engineering, manipulation of lattice-point defects is also essential for ZT improvement because these defects normally act as donors or acceptors of free electrons. For example, antisite defect (Bi_{Te}) and Bi vacancy (V_{Bi}) are acceptor-like defects, while Te_{Bi} and V_{Te} are donor-like defects. Individual concentration of these defects will be modulated to different degrees by the mechanical process and thermal treatment applied. Generally, Bi_{Te} is the dominant point defect in stoichiometric Bi_2Te_3 due to its low formation energy.[8−10] If Bi_2Te_3 is prepared by powder metallurgy, milling-induced fracture tends to occur along the basal plane between two $Te^{(1)}$ layers.[11−13] Hence, Te atoms with dangling bonds may escape more easily and leave vacancies behind, leading to an increase in V_{Te} concentration. In the subsequent pressing process the concentration of vacancy defects will be changed by dislocation gliding activity. The basal gliding has a major impact on V_{Te} defects, while the nonbasal one influences both V_{Te} and V_{Bi} with a concentration ratio of $[V_{Te}]/[V_{Bi}]$ equal to 3/2.[14] The dislocation-mediated vacancy annihilation mechanism has been successfully adapted to explain the change of carrier concentration for the Bi−Te compounds subject to plastic deformation and postannealing.[14,15] Once the vacancy concentration is oversaturated, the excess V_{Te} defects will be eliminated during thermal annealing due to their high mobility along basal planes and dislocation cores.[16]

Received: May 7, 2015
Published: July 22, 2015

DOI: 10.1021/acs.inorgchem.5b01031
Inorg. Chem. 2015, 54, 7438−7444

Among various Bi−Te-based compounds, $(Bi,Sb)_2Te_3$ and $Bi_2(Se,Te)_3$ are two representative P-type and N-type semiconductors used in commercial thermoelectric devices. For $Bi_2(Se,Te)_3$, Se addition would increase the probability of forming V_{Te} defects because Se atoms tend to occupy $Te^{(2)}$ sites and evaporate readily due to their low evaporation energy of ∼37.7 kJ/mol.[17] Control of V_{Te} concentration undoubtedly becomes an important task to optimize the thermoelectric properties of $Bi_2(Se,Te)_3$.[18,19] N-type $Bi_2(Se,Te)_3$ usually has inferior thermoelectric performance to P-type $(Bi,Sb)_2Te_3$ prepared by powder metallurgy.[7] Hu et al. have demonstrated that a repetitive hot deformation process can lead to a nearly 75% improvement in *ZT* value from 0.57 to 1 for $Bi_2(Se,Te)_3$ via crystallographic texture engineering.[20] Moreover, since re-evaporation of Te and Se elements is an important source of V_{Te} defects, a small compositional fluctuation would cause a large variation in carrier concentration for $Bi_2(Se,Te)_3$.[17] Halogen doping is an effective solution to the Te(Se) re-evaporation issue because halogens may take the Te sites and get ionized easily at room temperature.[21−23] An appropriate halogen doping can stabilize the crystal structure and minimize the batch-to-batch variation in electronic properties of $Bi_2(Se,Te)_3$. Group IB elements such as Ag and Cu are also common doping elements in Bi−Te-based compounds. Naravtil et al. have reported that $Te^{(1)}$ atoms in Bi_2Te_3 have a high negative charge and result in a strong repulsive force according to their theoretical computations.[24] Ag and Cu preferentially occupy the interstitial sites at the van der Waals gap between $Te^{(1)}$ layers by forming Ag_i defects.[24,25] Liu et al. have also suggested that the presence of Cu interstitials, Cu_i, improves the sample-to-sample variation in electronic properties of $Bi_2Te_{2.7}Se_{0.3}$ by suppressing V_{Te} formation.[17] However, the available interstitial sites at the van der Waals gap are limited, and excess Ag and Cu dopants may take Bi substitutional sites by forming Ag_{Bi} and Cu_{Bi} substitutional defects.[26,27] In summary, the combination of all vacancies and substitutional and interstitial defects have, without question, a rather complicated influence on thermoelectric properties of Ag-doped $Bi_2(Se,Te)_3$. However, we still lack a systematic study on the roles of various Ag-related lattice defects in $Bi_2(Se,Te)_3$. This study intends to investigate the electronic characteristics of Ag-related lattice defects and their influence on thermoelectric properties of $Bi_2(Se,Te)_3$ as functions of Ag doping content and thermal annealing temperature.

EXPERIMENTAL SECTION

N-type $Bi_2(Se,Te)_3$ compounds with various amounts of Ag were prepared by powder metallurgy followed by thermal annealing at different temperatures. First, pure Bi, Se, and Te elements with a stoichiometric composition of $Bi_2Se_{0.45}Te_{2.55}$ were melted in a quartz tube that was maintained at 860 °C. The solidified ingot was purified by a conventional zone-melting process at 740 °C with a rate of 12.5 mm/h. The purified $Bi_2(Se,Te)_3$ ingot was crushed into small chunks (<150 μm in particle size) and mixed with lab-grade Ag powders of ∼100 nm in size (99.9 wt %, CERAMET) for subsequent milling process. The mixture with different Ag contents (0, 0.2, 0.5, 1.0, and 3.0 wt %) was ground into fine powders (<2 μm) using a planetary ball miller (Retch, PM-100) at a speed of 300 rpm for 24 h. Next, the ground powders were pressed into a disk-shaped specimen (ϕ = 12.76 mm; thickness = 1 mm) under a pressure of 600 MPa at room temperature for 5 min. Finally, the cold-pressed specimens were thermally annealed at 250 and 350 °C for 2 h, respectively, under a vacuum pressure of ∼1×10^{-3} Torr.

Crystallographic structure and morphology of the pressed and annealed specimens were examined by an X-ray diffractometer (XRD, Shimadzu, LabX XRD-6000) with a Cu Kα line source and a scanning electron microscopy (SEM, Hitachi, SU8010). Seebeck measurements were performed at room temperature using a typical temperature-gradient approach.[28] The specimen was fixed on a homemade sample holder with a heater at one end to establish a small temperature gradient along the specimen. Both the temperature difference and the voltage across the specimen under a temperature gradient were measured using two T-type thermocouples in contact to the specimen. The Seebeck coefficient was then determined from the slope of the measured Seebeck voltage versus the temperature difference across the specimen. Electrical resistivity, carrier concentration, and carrier mobility were measured in the temperature range of 80−300 K using two different Hall effect measurement systems (ECOPIA, HMS-3000, and HMS-5000). Thermal diffusivity and mass density were measured at room temperature by a laser flash technique (NETZSCH, LFA 457) and an Archimedes method, respectively. The cold-pressed $Bi_2(Se,Te)_3$ specimens have a relative mass density of ∼90% of theoretical value, and no significant densification is observed after a pressureless sintering process. Heat capacity was measured by a differential scanning calorimetry analyzer (NETZSCH, DSC 200 F3Maia). The thermal conductivity of the specimens was then determined from the equation $\kappa = \rho_d \cdot C_p \cdot D$, where D, ρ_d ,and C_p are thermal diffusivity, mass density, and heat capacity, respectively.

RESULTS AND DISCUSSION

Compositional deviation and degradation of electronic properties are rather common scenarios for $Bi_2(Se,Te)_3$ compounds after high-temperature treatments due to re-evaporation of volatile constituents Se and Te. Microstructure and electronic properties of $Bi_2(Se,Te)_3$ compounds are easily dictated by the mechanical process and thermal treatment applied. Adding minute Ag element in $Bi_2(Se,Te)_3$ not only adjusts its thermoelectric properties but also raises its structural and electronic stability.[17,29] Before addressing the interactions between Ag and lattice defects in $Bi_2(Se,Te)_3$, we examined the crystallographic structure and electronic characteristics of $Bi_2(Se,Te)_3$ compounds to establish a reference for the Ag-doped $Bi_2(Se,Te)_3$ materials studied. Figure 1 shows the cross-sectional SEM images of as-pressed and thermally treated $Bi_2(Se,Te)_3$ specimens. The thermal annealings were performed at 250 and 350 °C for 2 h, respectively. The as-pressed sample shows a granular morphology with rough surfaces and blunt edges, which is apparently inherited from the powder morphology of milled $Bi_2(Se,Te)_3$. The granular structure has a feature size of 0.1−3 μm that is similar to the size of milled powders. It implies that the $Bi_2(Se,Te)_3$ powders were physically contacted only after cold-press operation. If the specimen was annealed at 250 °C, a few flatly cleaved surfaces as well as round-shaped granular structures are observed in the magnified SEM image of fractured surface of $Bi_2(Se,Te)_3$, as shown in the marked regions in Figure 1b. By increasing the annealing temperature to 350 °C, the specimen reveals a distinct fractural morphology with acute fragments and flatly cleaved surfaces. Generally, a large and flatly cleaved surface is only observed in zone-melted bismuth telluride compounds because fracture occurs preferentially along the crystallographic basal planes that are weakly bonded by van der Waals forces.[11−13] The observed fractural morphology suggests that the loosely joined $Bi_2(Se,Te)_3$ powders become chemically bonded after high-temperature annealing process. In addition to fractural morphology, some microstructural and crystallographic details of the as-pressed and annealed $Bi_2(Se,Te)_3$ specimens are further revealed by XRD analysis, as shown in Figure 2. The full width half maxima (fwhm) of major reflections appear to decrease with the increase of annealing

DOI: 10.1021/acs.inorgchem.5b01031
Inorg. Chem. 2015, 54, 7438−7444

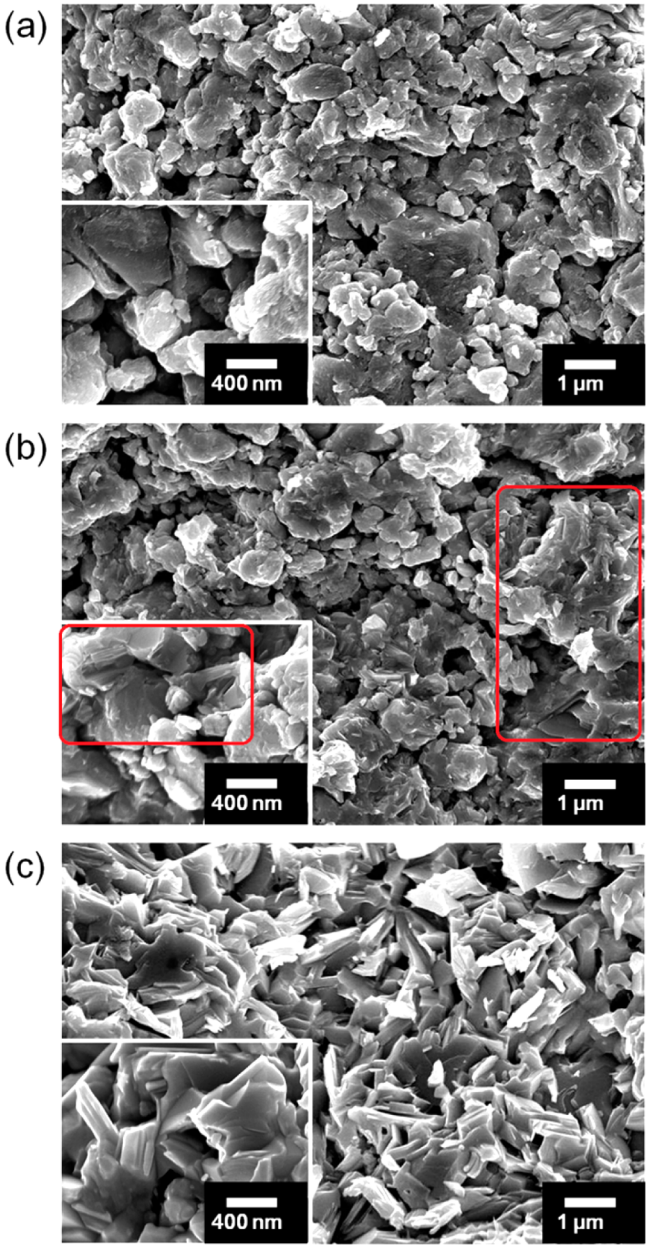

Figure 1. Cross-sectional SEM images of as-pressed and thermally annealed $Bi_2(Se,Te)_3$ specimens. (a) As-pressed. (b) Annealed at 250 °C. (c) Annealed at 350 °C.

temperature. Since $Bi_2(Se,Te)_3$ powders were subject to repeated fracture and mechanical deformation during milling and pressing processes, some residual strain and abundant electrically nonactive or active lattice defects would be introduced in the as-pressed $Bi_2(Se,Te)_3$ specimens. The diminishing fwhm is likely to be associated with the strain relaxation, and grain coalescence phenomena occurred in annealed $Bi_2(Se,Te)_3$ specimens.

Thermal annealing not only causes microstructural evolution but also changes concentrations of various lattice defects and, in turn, electrical transport properties of $Bi_2(Se,Te)_3$ compounds. Figure 3 shows the variation of carrier concentration and mobility of as-pressed $Bi_2(Se,Te)_3$ specimens against annealing temperature. The as-pressed sample possesses a carrier concentration of 6.1×10^{19} cm^{-3} and an extremely low carrier mobility (~10 $cm^2/(V\ s)$). Such a high carrier concentration is

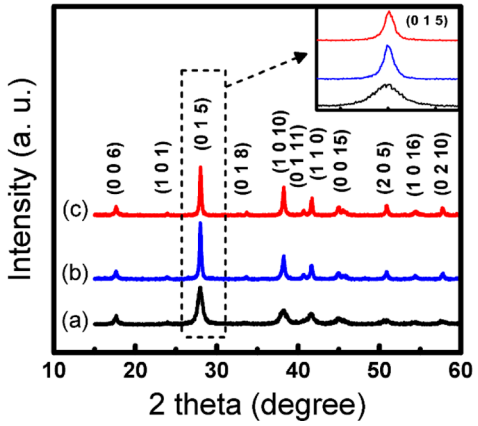

Figure 2. XRD patterns of as-pressed and thermally annealed $Bi_2(Se,Te)_3$ specimens. (a) As-pressed. (b) Annealed at 250 °C. (c) Annealed at 350 °C.

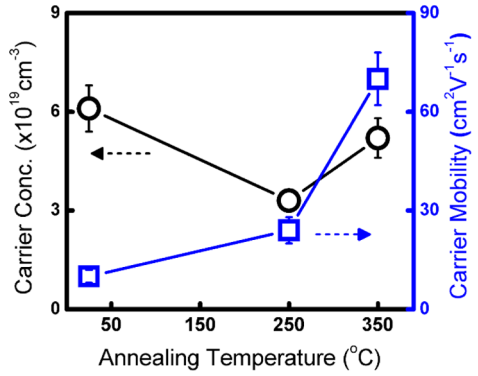

Figure 3. Variation of carrier concentration and mobility of nondoped $Bi_2(Se,Te)_3$ as a function of annealing temperature.

presumably attributed to abundant donor-like V_{Te} defects generated during high-energy milling process. After annealed at 250 °C, the $Bi_2(Se,Te)_3$ specimen has a carrier concentration reduced to 3.3×10^{19} cm^{-3} and a slightly increased mobility of 24 $cm^2/(V\ s)$. Strain recovery and defect elimination are believed to be held responsible for the change of electrical properties measured. It has been suggested that a climbing or gliding process may drive a dislocation to end on the $Te^{(1)}$ layer in bismuth telluride for minimization of free energy.[14,30] The dislocation climbing process toward low-energy $Te^{(1)}$ planes is accompanied by annihilation of donor-like V_{Te} defects that were generated abundantly during milling and pressing processes. Thus, the carrier concentration of $Bi_2(Se,Te)_3$ decreased after annealing at 250 °C. By increasing the annealing temperature to 350 °C, grain growth and surface sintering enable the annihilation of both V_{Bi} and V_{Te} defects through migration of grain boundaries and free surfaces. Since V_{Bi} is a triple-acceptor defect, the elimination of V_{Bi} would raise the electron concentration of $Bi_2(Se,Te)_3$ compounds. It explains why the carrier concentration of $Bi_2(Se,Te)_3$ is reduced after annealing at 250 °C and increased to 5.2×10^{19} cm^{-3} after annealing at 350 °C, as shown in Figure 3. However, the carrier mobility remains the increasing trend with annealing temperature because both V_{Te} and V_{Bi} are eliminated more easily at high temperature. It is worth mentioning that not only vacancy annihilation but also antisite defect formation may occur in the Bi−Te-based compounds during high-temperature annealing. For example, excess Bi atoms may combine with V_{Te}

DOI: 10.1021/acs.inorgchem.5b01031
Inorg. Chem. 2015, 54, 7438−7444

by forming Bi_{Te} defects. To study the influence of Ag doping on thermoelectric properties of $Bi_2(Se,Te)_3$, a thorough understanding of how Ag atoms interact with different lattice defects becomes essential.

Figure 4 shows the carrier concentrations of $Bi_2(Se,Te)_3$ samples with different Ag addition after annealing at 250 and

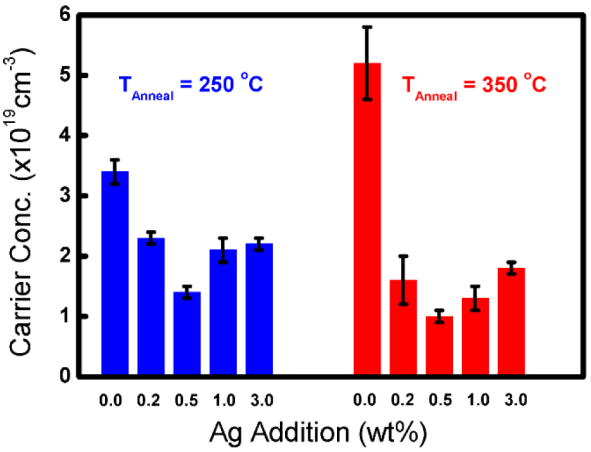

Figure 4. Carrier concentrations of $Bi_2(Se,Te)_3$ compounds with different Ag content and annealing temperatures.

350 °C for 2 h, respectively. The lightly doped samples (<0.5 wt % Ag) show decreasing carrier concentration with the increase of Ag content, while the heavily doped ones (>0.5 wt % Ag) reveal the opposite trend. The Ag-doped samples annealed at 350 °C obviously have slightly lower carrier concentrations than those annealed at 250 °C. It is worth mentioning that no diffraction peaks associated with any Ag-related heterogeneous phases were found in both lightly and heavily doped samples according to XRD analysis. Although very few Ag−Te precipitates of several micrometers in size were barely observed from the elemental mapping results (Supporting Information Figure S1), the influence of precipitates on carrier concentration is presumably small because these precipitates form scarcely and locally in Ag-doped $Bi_2(Se,Te)_3$. Thus, the observed changes of carrier concentration should be mainly attributed to the variations of lattice defect concentrations. Several defect mechanisms have been proposed to explain how Ag doping influences carrier concentration of Bi−Te-based compounds. One prevailing mechanism is that Ag atoms occupy the interstitial sites between $Te^{(1)}$ layers and provide free electrons.[24,25] However, the mechanism is contradictory to our measurement that the carrier concentration decreases with Ag addition in the range from 0 to 0.5 wt %. It has been suggested that the interstitial ions in the van der Waals gap may improve the mechanical properties of Bi−Te-based compounds by suppressing the formation of V_{Te}, as reported for Cu-doped Bi−Te compounds.[17] Following the above idea, if the presence of Ag_i raises the formation energy of V_{Te}, it would reduce the equilibrium concentration of V_{Te} and, in turn, the carrier concentration of the Ag-doped $Bi_2(Se,Te)_3$. The proposed interaction between Ag interstitial and V_{Te} is described below

$$Ag_s + xV_{Te}^{\bullet\bullet} + 2xe^- \rightarrow Ag_i^{\bullet} + e^- \quad (1)$$

where Ag_s stands for nonactivated Ag atoms residing at defect sources/sinks such as dislocations, grain boundaries, and interfaces. The coefficient "x" reflects how efficiently V_{Te} is suppressed by Ag_i. The higher the x value, the lower the equilibrium V_{Te} concentration. If $x > 0.5$, the number of free electrons annihilated is larger than that provided by Ag_i. Therefore, the carrier concentration decreases with increasing Ag addition for the lightly doped samples. However, the available interstitial sites in bismuth telluride are limited.[26,27] A further increase in Ag concentration would either remain at defect sources/sinks or form another type of lattice defect. It is speculated that Ag may combine with V_{Bi} by forming Ag_{Bi} substitutional defects as described below.

$$Ag_S + V_{Bi}''' + h^+ \rightarrow Ag_{Bi}'' \quad (2)$$

The net effect of forming an Ag_{Bi} defect would be the removal of a hole carrier, resulting in the increase of carrier concentration (electrons). It explains why the carrier concentration increases with Ag addition for the heavily doped samples, as shown in Figure 4. It is worth mentioning that the solubility limit of Ag_i in bismuth telluride may increase at high temperature. Therefore, an increased Ag_i concentration would further suppress V_{Te} formation and give rise to a lower carrier concentration, as shown in Figure 4.

The aforementioned lattice defects may change not only carrier concentrations but also lattice parameters of $Bi_2(Se,Te)_3$ compounds. The presence of Ag_i is expected to enlarge c-axis lattice parameter,[17] while that of Ag_{Bi} diminishes both a- and c-axis lattice parameters of Ag-doped $Bi_2(Se,Te)_3$ compounds due to distinct atomic sizes of Ag and Bi elements.[25] A careful analysis of XRD results may also shed light on the dominant defect type in the Ag-doped $Bi_2(Se,Te)_3$ compounds. The lattice constants a and c are calculated from the reflections of (0 0 6), (0 0 15), (0 1 5), (1 1 0), (1 0 10), (2 0 5) in the XRD patterns. Each lattice constant is obtained from one or two peaks, and the quality of data is evaluated by calculating the deviations from the mean value. The same calculation has been applied on the referenced Bi−Se−Te compounds (JCPDF Nos. 51−0643 and 50−0954). The deviation of lattice constants calculated for the Ag-doped $Bi_2(Se,Te)_3$ compounds studied is comparable to that of the referenced Bi−Se−Te compounds. Figure 5 shows the a- and c-axis lattice parameters against Ag content for the Ag-doped $Bi_2(Se,Te)_3$ compounds after annealing at 350 °C for 2 h. The a- and c-axes lattice parameters of $Bi_2Se_{0.5}Te_{2.5}$ compounds (JCPDF No. 51−0643) are also marked by dash lines for comparison. Basically, the a-axis lattice parameter of annealed $Bi_2(Se,Te)_3$ samples does not

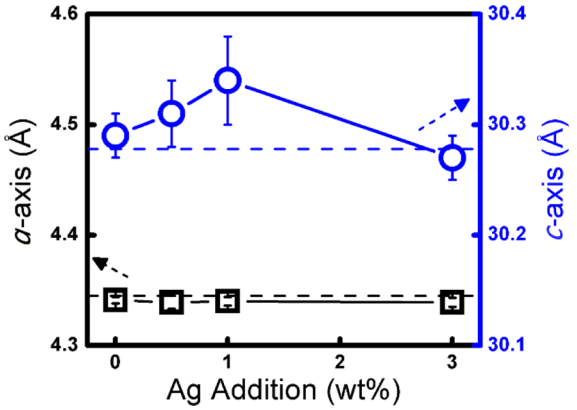

Figure 5. Variations of a- and c-axes lattice parameters of Ag-doped $Bi_2(Se,Te)_3$ annealed at 350 °C as a function of Ag addition.

DOI: 10.1021/acs.inorgchem.5b01031
Inorg. Chem. 2015, 54, 7438−7444

change significantly with the degree of Ag addition. However, the *c*-axis lattice parameter appears to increase with the increase of Ag content (0−1 wt %) and decreases with further increase in Ag content (3 wt % Ag). The increasing *c*-axis lattice parameter is presumably attributed to the increasing concentration of Ag_i in the Ag-doped samples (<1 wt % Ag). The trend indeed agrees with our hypothesis that the decrease of carrier concentration is caused by the increase of Ag_i concentration described in the previous section. It is worth mentioning that the x value in eq 1 may change with V_{Te} concentration. When V_{Te} concentration is high ($x > 0.5$), the formation of Ag_i is accompanied by the annihilation of V_{Te} and free electrons. The carrier concentration is expected to decrease with the increase of Ag_i concentration. Nevertheless, if V_{Te} has been eliminated to a low level, the annihilation efficiency of V_{Te} may decrease; that is, $x < 0.5$. Thus, the increasing Ag_i concentration may raise the carrier concentration of Ag-doped $Bi_2(Se,Te)_3$. It explains why the minimal carrier concentration is found at the lower Ag content (0.5 wt %), while the maximum *c*-axis lattice parameter is located at the higher Ag content (1 wt %). However, with further increase in Ag content (3 wt % Ag), the concentration of Ag_i reaches the limit of solubility, and some Ag atoms may combine with V_{Bi} by forming Ag_{Bi} substitutional defects that would diminish *c*-axis lattice parameter and raise carrier (electrons) concentration.

Ag-related lattice defects not only affect carrier concentration but also modulate electrical and thermal transport characteristics of $Bi_2(Se,Te)_3$ compounds. Figure 6 shows the carrier mobility, carrier concentration, and electrical resistivity of Ag-doped $Bi_2(Se,Te)_3$ compounds measured at the temperature (T) from 80 to 300 K. Note that the temperature dependence of carrier mobility is strongly correlated with scattering mechanism. Theoretically, the carrier mobility is proportional to $T^{-3/2}$ for acoustic phonon scattering and $T^{3/2}$ for ionized impurity scattering. If more than one scattering mechanism is involved, the effective carrier mobility (μ_{eff}) can be expressed as

$$\frac{1}{\mu_{eff}} = \frac{1}{\mu_{lattice}} + \frac{1}{\mu_{impurity}} + \cdots \quad (3)$$

where $\mu_{lattice}$ and $\mu_{impurity}$ stand for the carrier mobility with the dominant scattering sources to be lattice phonon and ionized impurity, respectively.[31] For the Ag-doped $Bi_2(Se,Te)_3$ specimens, the parameter n describing the temperature dependence of carrier mobility $\mu \propto T^n$ is found to change from −0.68 to −0.41 when the Ag content increases from 0.2 to 3.0 wt %. Obviously, the Ag-doped $Bi_2(Se,Te)_3$ samples have a mixed scattering mode with the n value ranging between −3/2 to 3/2 (n = −3/2: lattice scattering, n = 3/2: ionized impurity scattering). A less negative n value implies a more significant impurity scattering in the system. The mobility trend indeed agrees with our hypothesis that the concentration of Ag-induced defects increases with the increasing Ag content in the $Bi_2(Se,Te)_3$ specimens. Since the ionization energies of Ag_i and Ag_{Bi} are small in Bi−Te-based compounds,[25,26] all lattice defects have become ionized at the temperature above 80 K, and hence the carrier concentration does not change significantly with temperature for the Ag-doped $Bi_2(Se,Te)_3$ specimens (Figure 6b). The increasing trend of electrical resistivity is mainly associated with the decreasing trend of carrier mobility with increasing temperature for the Ag-doped $Bi_2(Se,Te)_3$ specimens (Figure 6c).

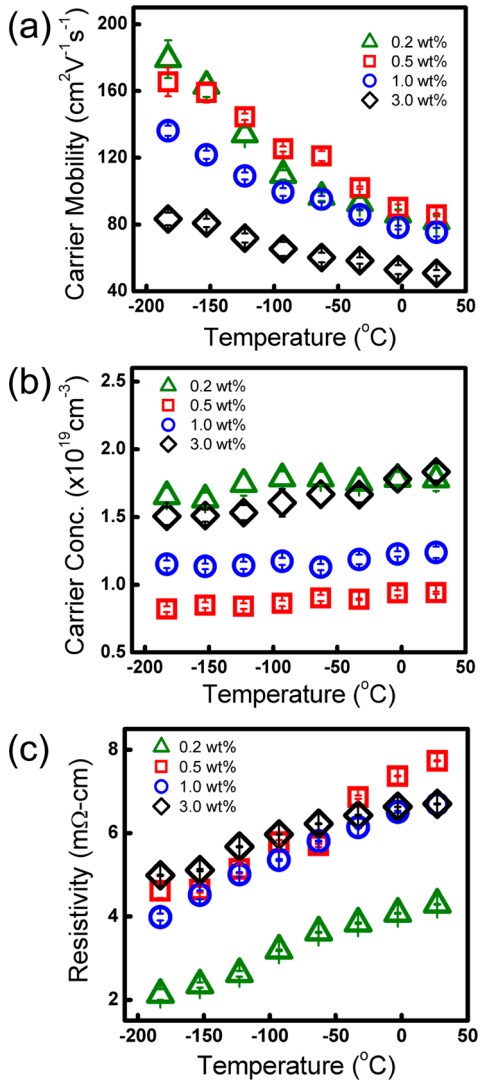

Figure 6. Temperature-dependent electrical transport properties of Ag-doped $Bi_2(Se,Te)_3$ with various Ag content. (a) Carrier mobility. (b) Carrier concentration. (c) Electrical resistivity.

According to classical Boltzmann transport theory, the carrier concentration and Seebeck coefficient of thermoelectric materials are expressed as[32]

$$n = \frac{4}{\sqrt{\pi}}\left(\frac{2\pi m_{eff}}{h^2}\right)^{3/2}\int_0^\infty E^{1/2} f \, dE \quad (4)$$

$$S = \frac{1}{eT}\left[E_F - \frac{\int_0^\infty E^{r+5/2}(\partial f(E)/\partial E)dE}{\int_0^\infty E^{r+3/2}(\partial f(E)/\partial E)dE}\right] \quad (5)$$

where m_{eff}, $f(E)$, and E_F are effective mass, Fermi−Dirac distribution function, and Fermi level, respectively. The scattering parameter r describes the energy dependence of the carrier relaxation time $\tau = \tau_0 E^r$ (r = −1/2: lattice scattering; r = 0: neutral impurity scattering; r = 3/2: ionized impurity scattering).[33] By assuming an approximate single-band model, the effective mass m_{eff} = 0.8 is chosen based on the fitting results of measured transport properties to eqs 4 and 5. Figure 7 shows the variation of Seebeck coefficient against carrier concentration for the $Bi_2(Se,Te)_3$ specimens measured at room temperature. The theoretical lines are calculated with different r

DOI: 10.1021/acs.inorgchem.5b01031
Inorg. Chem. 2015, 54, 7438−7444

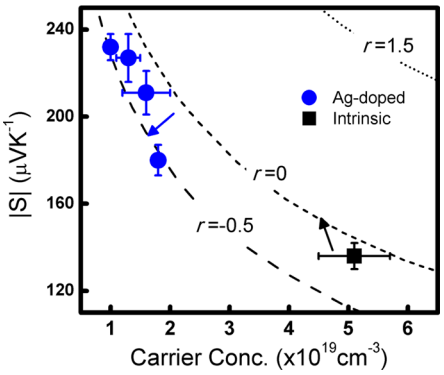

Figure 7. Experimental and theoretical Seebeck coefficients of intrinsic and Ag-doped $Bi_2(Se,Te)_3$ as a function of carrier concentration.

values that reflect specific scattering mechanism. The experimental data are mainly located between the theoretical predictions with $r = -1/2$ and $r = 0$. It suggests that the carriers are scattered by both phonons and impurities at room temperature in the $Bi_2(Se,Te)_3$ samples studied. It is interestingly noted that the data of Ag-doped specimens are closer to the $r = -1/2$ prediction because great portions of V_{Te} and V_{Bi} defects are annihilated at elevated temperatures with the presence of Ag dopants in $Bi_2(Se,Te)_3$. However, the data of intrinsic $Bi_2(Se,Te)_3$ appear to deviate slightly toward the $r = 0$ prediction since more residual vacancy defects become active scattering sources for charge carriers. Generally, the Ag-doped $Bi_2(Se,Te)_3$ specimens have a larger Seebeck coefficient and lower carrier concentration than the intrinsic $Bi_2(Se,Te)_3$ specimens.

Besides electrical transport properties, thermal conductivity of Ag-doped $Bi_2(Se,Te)_3$ compounds is also affected by the electrical conductivity and lattice distortion caused by Ag-induced lattice defects. Figure 8 shows the electronic thermal

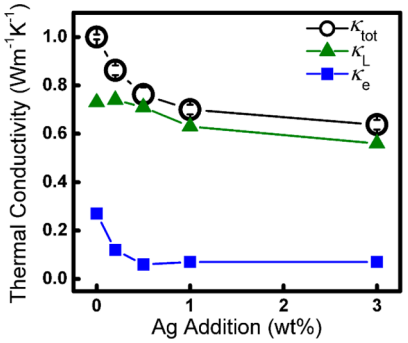

Figure 8. Variations of electronic thermal conductivity, lattice thermal conductivity, and total thermal conductivity of Ag-doped $Bi_2(Se,Te)_3$ compounds annealed at 350 °C as a function of Ag addition.

conductivity (κ_e), lattice thermal conductivity (κ_L), and total thermal conductivity (κ_{tot}) of the Ag-doped $Bi_2(Se,Te)_3$ compounds annealed at 350 °C as a function of Ag addition. The electronic thermal conductivity was calculated from the measured electrical conductivity according to the Wiedmann–Franz relation $\kappa_e = L\sigma T$, with $L = 1.6 \times 10^{-8}$ $W\Omega/K^2$ determined from the measured transport properties. A significant decrease in κ_e in the lightly doped specimens (<0.5 wt % Ag) is believed to be associated with the decrease of carrier concentration resulting from formation of Ag_i defects. With further increase in Ag content, no marked change in κ_e was observed because carrier concentration and, in turn, electrical conductivity do not change notably in this doping range. However, the increasing degree of lattice distortion caused by Ag-induced lattice defects would lead to a decrease in κ_L, especially for the heavily doped specimens (>0.5 wt % Ag).

In summary, the Ag-doped $Bi_2(Se,Te)_3$ has a higher Seebeck coefficient, a larger electrical resistivity, and a lower thermal conductivity than the pristine $Bi_2(Se,Te)_3$ studied. An approximate 10% enhancement of ZT value from 0.30 to 0.34 at room temperature was achieved for the 1 wt % Ag-doped $Bi_2(Se,Te)_3$. The $Bi_2(Se,Te)_3$ samples do not have very attractive ZT values due mainly to their low mass density (~90% of theoretical value) and, in turn, high electrical resistivity. The relative density of $Bi_2(Se,Te)_3$ indeed can be improved to 99% easily by a hot-press method. The understanding obtained regarding Ag-related lattice defects in bismuth telluride shall facilitate the development of quality thermoelectrics by tweaking defect concentration and carrier scattering mechanism through appropriate doping process.

CONCLUSIONS

In this study the interactions between Ag and various lattice defects in $Bi_2(Se,Te)_3$ compounds are systematically investigated. It is found that interstitial Ag_i and substitutional Ag_{Bi} are two major types of lattice defects that modulate the electrical and thermal transport properties of Ag-doped $Bi_2(Se,Te)_3$ compounds. The presence of Ag_i defects reduces the equilibrium concentration of V_{Te} defects and leads to a decreased carrier concentration with increasing Ag content in $Bi_2(Se,Te)_3$. When more Ag atoms are added in the $Bi_2(Se,Te)_3$ compound, the increasing concentration of Ag_{Bi} defects is held responsible for the increase of electron concentration because Ag_{Bi} formation is accompanied by hole removal. The change of dominant lattice defect type is also reflected by the variation of c-axis lattice parameters of the Ag-doped $Bi_2(Se,Te)_3$. The Seebeck coefficients and temperature-dependent electrical properties suggest that the Ag-doped $Bi_2(Se,Te)_3$ compounds have a mixed scattering mechanism for charge carriers. This study provides a doping strategy for simultaneous control of electrical and thermal transport properties of bismuth telluride through manipulating Ag-related lattice defects.

ASSOCIATED CONTENT

Supporting Information

Elemental mapping results of Ag-doped $Bi_2(Se,Te)_3$ from field-emission electron-probe microanalysis. The Supporting Information is available free of charge on the ACS Publications website at DOI: 10.1021/acs.inorgchem.5b01031.

AUTHOR INFORMATION

Corresponding Author

*E-mail: cnliao@mx.nthu.edu.tw.

Notes

The authors declare no competing financial interest.

ACKNOWLEDGMENTS

The work is supported by Ministry of Science and Technology of Taiwan through Grant MOST 103-2221-E-007-035. Partial financial support from Industrial Technology Research Institutes and China Steel Corporation are also acknowledged.

DOI: 10.1021/acs.inorgchem.5b01031
Inorg. Chem. 2015, 54, 7438–7444

REFERENCES

(1) Bell, L. E. *Science* **2008**, *321*, 1457−1461.
(2) Niu, X.; Yu, J.; Wang, S. *J. Power Sources* **2009**, *188*, 621−626.
(3) Caillat, T.; Carle, M.; Pierrat, P.; Scherrer, H.; Scherrer, S. *J. Phys. Chem. Solids* **1992**, *53*, 1121−1129.
(4) Yan, X.; Poudel, B.; Ma, Y.; Liu, W. S.; Joshi, G.; Wang, H.; Lan, Y.; Wang, D.; Chen, G.; Ren, Z. F. *Nano Lett.* **2010**, *10*, 3373−3378.
(5) Ashida, M.; Hamachiyo, T.; Hasezaki, K.; Matsunoshita, H.; Kai, M.; Horita, Z. *J. Phys. Chem. Solids* **2009**, *70*, 1089−1092.
(6) Jiang, J.; Chen, L.; Bai, S.; Yao, Q.; Wang, Q. *Mater. Sci. Eng., B* **2005**, *117*, 334−338.
(7) Shen, J. J.; Hu, L. P.; Zhu, T. J.; Zhao, X. B. *Appl. Phys. Lett.* **2011**, *99*, 124102.
(8) Miller, G. R.; Li, C. Y. *J. Phys. Chem. Solids* **1965**, *26*, 173−177.
(9) Stary, Z.; Horak, J.; Stordeur, M.; Stolzer, M. *J. Phys. Chem. Solids* **1988**, *49*, 29−34.
(10) Kim, D. H.; Kwon, I. H.; Kim, C.; Han, B.; Im, H.-J.; Kim, H. *J. Alloys Compd.* **2013**, *548*, 126−132.
(11) Im, J. K.; Hartwig, K. T.; Sharp, J. *Acta Mater.* **2004**, *52*, 49−55.
(12) Chen, Z. C.; Suzuki, K.; Miura, S.; Nishimura, K.; Ikeda, K. *Mater. Sci. Eng., A* **2009**, *500*, 70−78.
(13) Lin, S. S.; Liao, C. N. *J. Appl. Phys.* **2011**, *110*, 093707.
(14) Schultz, J. M.; Mchugh, J. P.; Tiller, W. A. *J. Appl. Phys.* **1962**, *33*, 2443−2450.
(15) Balluffi, R. W.; Allen, S. M.; Cater, W. C. *Kinetics of Materials;* Wiley: Hoboken, NJ, 2005; pp 253−283.
(16) Lu, M. P.; Liao, C. N. *J. Alloys Compd.* **2013**, *571*, 178−182.
(17) Liu, W. S.; Zhang, Q.; Lan, Y.; Chen, S.; Yan, X.; Zhang, Q.; Wang, H.; Wang, D.; Chen, G.; Ren, Z. *Adv. Energy Mater.* **2011**, *1*, 577−587.
(18) Horak, J.; Star, Z.; Votinsk, J. *Philos. Mag. B* **1994**, *69*, 31−38.
(19) Horak, J.; Stary, Z.; Lostak, P.; Pancir, J. *J. Phys. Chem. Solids* **1990**, *51*, 1353−1360.
(20) Hu, L. P.; Liu, X. H.; Xie, H. H.; Shen, J. J.; Zhu, T. J.; Zhao, X. *Acta Mater.* **2012**, *60*, 4431−4437.
(21) Goldsmid, H. J. *Proc. Phys. Soc., London* **1958**, *71*, 633−646.
(22) Yamashita, O.; Tomiyoshi, S. *Jpn. J. Appl. Phys.* **2003**, *42*, 492−500.
(23) Perrin, D.; Chitroub, M.; Scherrer, S.; Scherrer, H. *J. Phys. Chem. Solids* **2000**, *61*, 1687−1691.
(24) Bludska, J.; Jakubec, I.; Drasar, C.; Lostak, P.; Horak, J. *Philos. Mag.* **2007**, *87*, 325−335.
(25) Navratil, J.; Klichova, I.; Karamazov, S.; Sramkova, J.; Horak, J. *J. Solid State Chem.* **1998**, *140*, 29−37.
(26) Chizhevskaya, S. N.; Shelimova, L. E. *Inorg. Mater.* **1995**, *31*, 1083−1095.
(27) Yang, J.; Chen, R.; Fan, X.; Bao, S.; Zhu, W. *J. Alloys Compd.* **2006**, *407*, 330−333.
(28) Testardi, L. R.; McConnell, G. K. *Rev. Sci. Instrum.* **1961**, *32*, 1067−1068.
(29) Zhang, X.; Ma, X. Y.; Lu, Q. M.; Zhang, F. P.; Liu, Y. Q.; Zhang, J. X.; Wang, L. *J. Electron. Mater.* **2011**, *40*, 773−777.
(30) Delavignette, P.; Amelinckx, S. *Philos. Mag.* **1961**, *6*, 601−608.
(31) Seeger, K. *Semiconductor Physics: An Introduction;* Springer: New York, 2004; pp 159−174.
(32) Nolas, G. S.; Sharp, J.; Goldsmid, H. J. *Thermoelectrics: Basic Principles and New Materials Developments;* Springer: New York, 2001; pp 36−44.
(33) Lundstrom, M. *Fundamentals of Carrier Transport;* Cambridge University Press: New York, 2000; pp 64−67.

DOI: 10.1021/acs.inorgchem.5b01031
Inorg. Chem. 2015, 54, 7438−7444